PAPER • OPEN ACCESS

Characterization of the thermal conductivity and diffusivity of graphene nanoplatelets strips: a low-cost technique

To cite this article: G Giovinco *et al* 2023 *Nanotechnology* **34** 345703

View the article online for updates and enhancements.

Characterization of the thermal conductivity and diffusivity of graphene nanoplatelets strips: a low-cost technique

G Giovinco[1] , S Sibilia[2,3] and A Maffucci[2,3,4]

[1] Department of Civil and Mechanical Engineering, University of Cassino and Southern Lazio, Via G. Di Biasio 43, I-03043 Cassino, FR, Italy
[2] Department of Electrical and Information Engineering, University of Cassino and Southern Lazio, Via G. Di Biasio 43, I-03043 Cassino, FR, Italy
[3] E-lectra srl, via Ponte La Pietra, I-03043 Cassino, FR, Italy
[4] INFN-Laboratori Nazionali di Frascati, via E. Fermi 40, I-00044 Frascati, RM, Italy

E-mail: giovinco@unicas.it

CrossMark

Abstract

This paper proposes a new technique to characterize the thermal conductivity and diffusivity of thin strips made by graphene nanoplatelets (GNP). The evaluation of these parameters is essential for a reliable design of thermal and electrothermal applications of graphene and is usually performed by means of assessed but expensive techniques such as those based on Raman effects and laser flash. The technique proposed here is simpler and less demanding in terms of equipment, and combines the results of an experimental characterization of the strip heated by the Joule effect obtained with infrared camera, with those provided by an electro-thermal model. Specifically, the evaluation of the thermal conductivity and diffusivity is the result of the analysis of the transient behavior of the measured and simulated solutions. The methodology is here successfully validated by applying it to commercial graphene strips and benchmarking against the thermal parameters provided by the manufacturers. Then, a complete characterization is provided for commercial strips based on different formulations of GNP and binders such as polyurethane, epoxy resin, and boron nitride. For these materials, the values of thermal conductivity and diffusivity are found in the ranges $(50\text{–}450)\,\mathrm{W\,m^{-1}\,K^{-1}}$ and $(0.5\text{–}3.5) \times 10^{-4}\,\mathrm{m^2\,s^{-1}}$, respectively.

Keywords: graphene nanoplatelets, electrothermal modeling, thermal conductivity, thermal diffusivity

(Some figures may appear in colour only in the online journal)

1. Introduction

Graphene-related materials have been extensively studied in view of their outstanding electro-thermal behavior [1, 2]. This suggested their use in a large variety of applications, such as thermo-electrical actuators [3–6] or sensors [7–9], as well as smart coatings or novel heat management systems [10–12]. For such reasons, it is of paramount importance assessing reliable and fast characterization techniques able to accurately estimate the electro-thermal properties associated with such novel materials, such as the electrical and thermal conductivity, the thermal emissivity, and so on.

A high thermal conductivity results in a faster pace for conducting heat. The studies of graphene-related materials have so far demonstrated some important facts (e.g. [13]): (i) materials based on graphene are characterized by a high thermal conductivity, as are materials like copper, natural

diamonds, silver, gold, etc; (ii) the thermal conductivity is an increasing function of the volume fraction of the nanoparticles; (iii) the thermal conductivity is also affected by the size of the nanoparticles.

In the last decades, extremely accurate models and experimental techniques have been proposed to characterize high-quality graphene-based materials, such as mono- or few- layer graphene sheets, perfectly aligned carbon nanotubes, and so on. As a consequence, the electrothermal properties of these materials can be considered well assessed in the literature, e.g. [14–19].

More recently, however, attention has been focused on the so-called poor-quality graphene-based materials, being the high-quality ones still unrealistic for many industrial applications due to the high costs that would be associated with their mass production given the presently available fabrication technologies. Therefore, alternative and cheaper materials are investigated, like composites including carbon-based reinforcements, that can be graphene flakes, carbon nanotubes, bucky-balls, and so on. A comprehensive review of such low-cost versions of graphene, comparing costs and performance, is provided in [20]. It is shown that a good trade-off between good physical properties, large-scale production, and reasonable costs, can be found in the materials based on graphene-nanoplatelets (GNPs). The GNPs look like irregular flakes of few-layer graphene [21] and can be fabricated with several industrially-scalable techniques such as: microwave irradiation [22, 23], ball-milling [24] or wet-jet milling [25].

The GNP materials investigated in this paper are macroscopic strips characterized by a high percentage of GNPs, with two dimensions of the order of cm and the third one (thickness) of the order of fractions of mm. These GNP films are proposed for realizing heating elements in several applications, like industrial ovens or de-icing systems.

In [26, 27] these materials have been studied and it has been assessed a technique to evaluate their temperature-dependent electrical conductivity and their thermal emissivity. In this paper, the study is extended to the thermal conductivity and to the thermal diffusivity in order to give a complete analysis and characterization of these GNP-based strips.

Specifically, this paper proposes a low-cost and easy technique to characterize such properties that can provide reliable results compared to the reference techniques so far adopted, at least in a significant range of values. The paper refers hereafter to the in-plane properties that are of great interest for the above-mentioned industrial applications. Indeed, due to their strong anisotropy, these strips exhibit off-plane values of such properties that can be orders of magnitude far from the in-plan ones.

A classical technique to characterize the in-plane thermal conductivity and diffusivity is based on opto-thermal Raman spectroscopy [16–18, 28, 29]. The main advantages of such techniques are, above all:

 (i) No need for sample preparation;
 (ii) Extremely quick (seconds) acquisition time for Raman spectra;
(iii) Possibility of transmitting the laser light and Raman

scattered light by optical fibers over long distances for remote analysis
(iv) Possibility to measure also the thermal diffusivity by using laser flash Raman spectroscopy.

On the other hand, the Raman effect is very weak, therefore requiring a sensitive and highly optimized instrumentation. Moreover, the fluorescence of impurities on the sample surface can hide the Raman spectrum. In addition, heating through intense laser radiation can damage the sample or cover the Raman spectrum. Last but not least, the experimental setup can be very expensive.

In order to overcome the above-mentioned disadvantages and to design an experimental setup that can be generalized to a very wide range of materials, alternative techniques have been proposed, such as the so-called laser-flash technique [30, 31]. Indeed, this is a technique applied for evaluating thermal diffusivity [32] that has become standard [33]. In this case, the thermal conductivity and diffusivity are obtained from an unsteady measurement technique. Specifically, the procedure consists of irradiating a surface of the GNP sample and measuring the temperature increase on the opposite side, preferably with a contact-less thermometer, such as a pyrometer or an infrared (IR) camera. The method requires a pulsed thermal source, usually a photographic flash or a laser.

The most important disadvantages are the following:

 (i) A very short energy pulse can produce a meaningful temperature increase on the irradiated surface, which can even damage it;
 (ii) The technique is particularly suited for homogeneous and isotropic materials, which are not the case with GNP films (corrections must be applied to handle non-homogeneous and non-isotropic samples);
(iii) The sample illumination must be as uniform as possible;
(iv) In this case, too, the costs of the setup can be high.

The above-mentioned drawbacks of the standard characterization techniques suggest the investigation of alternative procedures. For instance, recent work [34] proposes to measure the thermal conductivity of carbon nanotube samples by using a pulsed photothermal reflectance technique and a four-layer heat conduction model based on the transmission-line theory.

In the same stream, the present paper proposes an alternative methodology to measure both the thermal diffusivity and conductivity of GNP strips, only based on the analysis of the spatio-temporal distribution of the temperature over the strip. Specifically, after heating by the Joule effect, the temperature distributions over the strips are both measured by means of an IR camera and simulated by means of a simple electro-thermal model. The proposed technique retrieves the thermal diffusivity and conductivity based on a joint analysis of the simulated and measured results. Besides the use of equipment that is much cheaper than standard techniques, another advantage of the proposed methodology resides in its simplicity of implementation.

The paper is organized as follows. The methodology is detailed in section 2, after a brief description of the industrial-
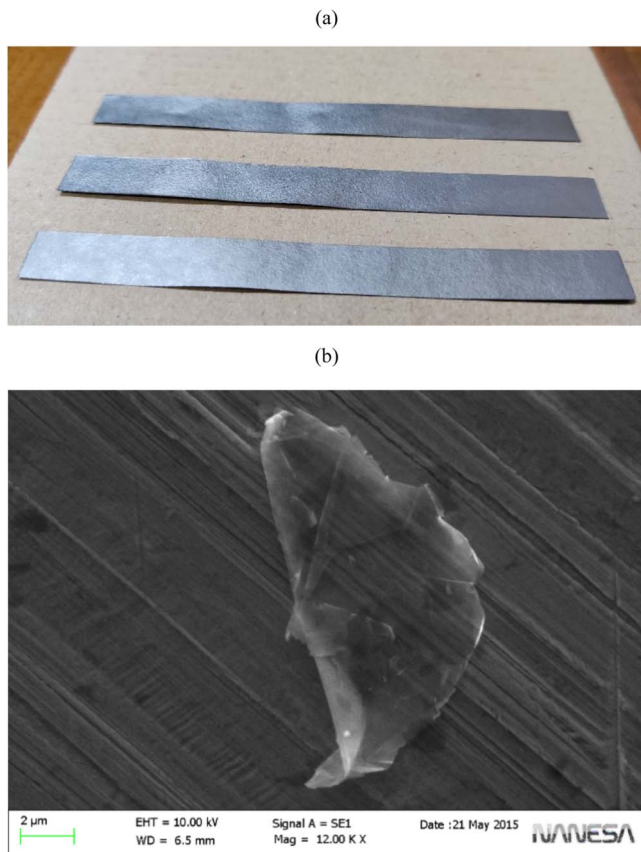
(a)

(b)

Figure 1. (a): The GNP strips under investigation (by NANESA); (b) SEM image of a single flake (the scale is 2 μm).

grade GNP strips adopted here (fabrication and characterization). In section 3, the method is first validated against two commercial materials with known parameters, then applied to characterize several kinds of GNP strips. Conclusions are drawn in section 4.

2. Methods and materials

2.1. Industrial strips of graphene nanoplatelets (GNP)

The graphene strips used in this work are freestanding, paper-like commercial materials, from different manufacturers. A picture of some of the strips produced by Nanesa srl [35] is provided in figure 1(a): their planar dimensions are 1 cm × 10 cm. The basic components of such strips are GNP flakes, as shown in the scanning electron microscope picture in figure 1(b). The GNPs are produced by Nanesa by using a proprietary liquid exfoliation technology, starting from graphitic precursors. The flakes are characterized by an average lateral dimension of about 30 μm, and an average thickness of about 14 nm, corresponding to about 40 graphene layers. The dimensions and the high aspect ratio provide such GNPs with interesting barrier properties, while their structure makes them excellent thermal and electric conductors. A Raman spectroscopy characterization (see figure 2) shows a low intensity and broadness of the D-band and a high intensity
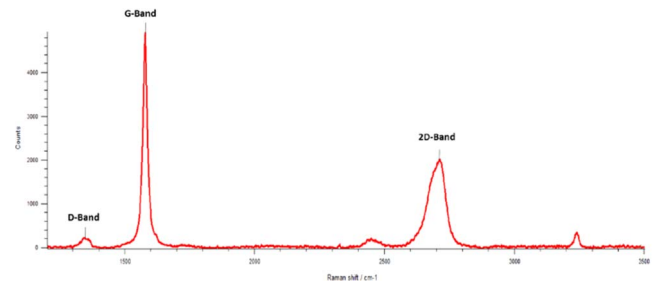

Figure 2. Raman spectroscopy characterization of the GNPs, highlighting a low intensity of the D band and a high intensity of the G band.

and sharpness of the G-band, therefore demonstrating that this industrial GNP has a low concentration of defects.

The GNPs are then mixed at different percentages (from 25% to 100%) with polymeric binders to realize the strips in figure 1(a). The process is carried out by means of a semi-automatic spraying system with an automatic plotter and a spray nozzle. Different deposition types are possible, either based on solvent or aqueous dispersions. The final thickness/ alignment ratio is optimized by a calendaring process. The characteristics of the GNP strips analyzed in this paper are listed in table 1: they differ in the type of binder, in the percentage of GNP, in the thickness, and in the annealing temperature.

As a general comment, the pure GNP strip (hereafter named G-paper) has the best thermal and electrical properties, whereas the G-Preg ones are more stable from a mechanical point of view and better interact with other polymers or composites.

Two GNP strips of comparable dimensions, produced by Panasonic and Graphtech, whose specifications are provided in section III, have been utilized to validate the suggested methodology.

2.2. Setup and models for the electrothermal characterization

The classical relation between the thermal diffusivity, *a* and the thermal conductivity, *k,* reads as follows [36]:

$$a = \frac{k}{\rho c}, \qquad (1)$$

where ρ is the density and *c* is the specific heat of the material.

The proposed methodology aims at measuring *k* and the product ρc so that the diffusivity *a* comes from (1). To this end, the simple set-up of figure 3 is proposed, where a graphene strip is heated by the Joule effect due to the flow of a suitable electrical current, and the distribution in space and time of the temperature over the strip is read by an IR camera. The strip is mounted on a test-fixture (figure 4), allowing the strips to free-stand, and equipped with two electrodes for imposing the electrical current. The fixture is placed inside a black hollow chamber.
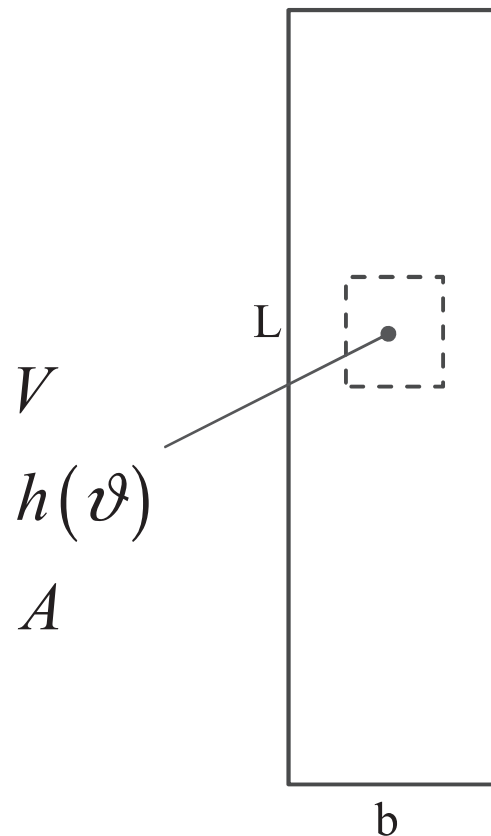
Being the graphene strips very thin (the thickness is lower than 100 μm, see table 1), the thermal gradient across the thickness can be neglected without significant errors. On the other hand, it is well known that 2D materials like graphene exhibit an in-plane conductivity much higher (2–3

Table 1. Characteristics of the GNP strips manufactured by NANESA studied in this paper.

Material	GNP%	Binder	Annealing T (°C)	Thickness δ (μm)
G-paper	100	—	—	74
G-Preg (95/5)	95	Polyurethane	200	75
G-Preg (80/20)	80	Polyurethane	200	75
G-Preg (70/30)	70	Epoxy resin	180	78
G-Preg (50/50)	50	Boron nitride	150	100
G-Preg (30/70)	30	Boron nitride	150	65
G-Preg (25/65-10)	25	Boron nitride-epoxy resin	180	75
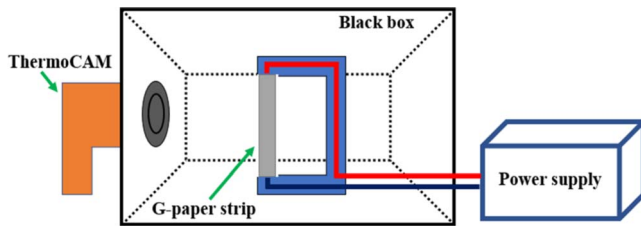
Figure 3. Schematic measurement setup for the evaluation of the thermal diffusivity of the GNP strips under investigation.

Figure 4. Picture of the measurement setup: a GNP strip is mounted on the test-fixture, inside the black box.

Figure 5. Small region of the strip where the temperature is uniform.

2.3. Methodology for estimating the thermal conductivity and diffusivity

The methodology proposed here is a two-step technique: in the first step, the quantity ρc was evaluated, being ρ the density and c the specific heat of the material. The second step provided an estimation of k. The thermal diffusivity was then derived by applying (1).

The first step started with the identification of a small volume of the GNP strip (of area A and thickness δ), where the temperature distribution can be assumed as uniform (see figure 5). Note that the temperature associated with each pixel of the IR image is the mean temperature of the pixel area, and thus the proposed methodology requires the choice of a pixel area much larger than that of the single GNP. The IR camera detector resolution is 640 × 480 pixels. The pixel area is about 0.5 mm × 0.5 mm, much larger than that of the single platelet (about 30 μm × 30 μm), and wide enough to

orders of magnitude or more) than the off-plane one [36]. Therefore, given the assumptions, the proposed methodology provides the value of the equivalent isotropic thermal conductivity of the graphene film that can be associated with its in-plane components.

include the presence of both binder and nanoplatelets. Since the IR camera thermal sensitivity (NETD) is about 0.05 °C, in the following, the temperature is assumed to be uniform if the maximum temperature gradient module is lower than 0.1 °C/pixel.

In such a region A, the radiative and convective heat transfer can be assumed to be much higher than the conductive one, and thus the following heat balance relation holds [37]:

$$\rho c V \frac{\partial T(\vartheta)}{\partial \vartheta} = 2A[h(\vartheta)(T(\vartheta) - T_\infty) + \sigma \varepsilon \cdot (T^4(\vartheta) - T_w^4)], \quad (2)$$

where V is defined as $V = A\delta$, $h(\vartheta)$ is the convective heat transfer coefficient, and σ and ε are the Stefan–Boltzmann constant and the thermal emissivity, respectively. In addition, T is the volume temperature, T_∞ is the surrounding air temperature and T_w is the mean radiant temperature of the surroundings.

The experiment proceeded as follows: the strip was electrically heated by the Joule effect with a controlled current until the desired temperature was reached, then the current was interrupted and a thermal transient took place. The transient evolution of the temperature (decay) allowed estimating the desired quantity ρc by numerically solving the differential equation (2) and minimizing the following error function:

$$E^2 = \sum_{\vartheta=0}^{\vartheta=\vartheta_{max}} (T(\vartheta) - \tilde{T}(\vartheta))^2, \quad (3)$$

where $\tilde{T}(\vartheta)$ was the measured temperature value. The following initial conditions were assumed: $T(\vartheta = 0) = \tilde{T}(\vartheta = 0)$. Note that the solution of model (2)–(3) required a preliminary estimation of the emissivity ε of the tested strips. This was carried out according to the procedure described in [26] and also applied in [27]. Specifically, the emissivity was identified by varying its value until an agreement was reached between the temperature values measured by the IR camera and those given by the contact thermocouples placed on the surface of the strip.

Once the product ρc was estimated, the thermal conductivity k was calculated through the second step of the methodology, consisting of the solution of the Fourier equation:

$$\rho \cdot c \cdot \delta \cdot \frac{\partial T}{\partial \vartheta} = k \cdot \delta \cdot \frac{\partial^2 T}{\partial y^2} + 2 \cdot [h \cdot (T_\infty - T)$$
$$+ \sigma \cdot \varepsilon \cdot (T_w^4 - T^4)] + Q, \quad (4)$$

where Q is the source related to the Joule effect. Indeed, equation (4) was discretized by applying the finite differences (FD) method with the 1D domain discretization shown in figure 6, leading to the following numerical equation at the
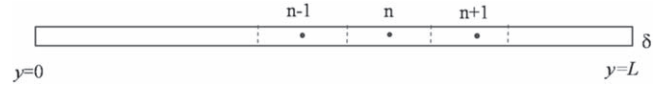

Figure 6. Domain discretization of the GNP strip in view of the evaluation of k through a finite difference method.

generic nth node [38]:

$$\rho \cdot c \cdot V_n \cdot \frac{T_n(\vartheta + 1) - T_n(\vartheta)}{\Delta \vartheta}$$
$$= k \cdot \delta \cdot w \cdot \frac{T_{n-1}(\vartheta) - T_n(\vartheta)}{\Delta y}$$
$$+ k \cdot \delta \cdot w \cdot \frac{T_{n+1}(\vartheta) - T_n(\vartheta)}{\Delta y}$$
$$+ 2 \cdot A_n \cdot [h_n(\vartheta) \cdot (T_\infty(\vartheta) - T_n(\vartheta))$$
$$+ \varepsilon \cdot \sigma \cdot (T_w^4(\vartheta) + - T_n^4(\vartheta))] + \Delta R_n(\vartheta) \cdot I^2, \quad (5)$$

where $A_n = w \cdot \Delta y$ and $V_n = A_n \cdot \delta$. Here, w is the discretization step in the lateral direction of the strip of width b and δ is the strip thickness, as detailed in the next subsection.

Moreover: h_n is the convective coefficient, ΔR_n is the electrical resistance of the nth sub-strip, T_∞ is the air temperature, T_w is the radiative equivalent temperature of the cavity, and I is the current flowing into the strip.

Denoting with $\tilde{T}$ the temperature of each pixel measured by means of the IR camera, the boundary conditions were:

$$T_1(\vartheta \geqslant 0) = \tilde{T}_1(\vartheta \geqslant 0),$$
$$T_N(\vartheta \geqslant 0) = \tilde{T}_N(\vartheta \geqslant 0), \quad (6)$$

where N was the total number of sub-strips.

The equivalent value of the conductivity, k, was then obtained through the minimization of the sum of the squared errors:

$$\epsilon^2 = \sum_{n=2}^{N-1} (T_n(\vartheta) - \tilde{T}_n(\vartheta))^2 \quad (7)$$

taking into account that the $\rho \cdot c$ product was already estimated.

The measurement procedure to impose (7) was carried on until steady conditions were almost reached (at least ten minutes in the present study). Note that the dependence on T of the electrical resistance ΔR_n of the nth sub-strip was estimated on the basis of the procedure reported in [27, 39].

Note that the equivalent thermal conductivity k identified here also includes the contributions of the thermal interfacial resistances associated with the single GNPs in the strip since the pixel area is much larger than that of a single GNP. In addition, the choice of analyzing an area of the strip far enough from the strip ends (see figure 5) allows us to consider as negligible the effect of the thermal interfacial resistances occurring at the terminal electrode/strip contact region.

2.4. Numerical implementation of the models

The details of the numerical implementation of the above models are provided in the following. The differential equations (2) and (5) were solved by means of the FD method by using a fully explicit scheme (Crank–Nicholson method).

Being the frame rate of the IR camera equal to 9 Hz, a time step of $1/900$ s was assumed, which is $1/100$ of the period. In addition, the temperature decay was considered in an interval of about $1/3$ s, in order to avoid that the heat exchange started to occur also in the planar directions.

For the IR frame corresponding to the time at which the electric source was shut down ($\vartheta = 0$), the following algorithm was applied to identify the uniformity region A described before (see figure 5):

- Step 1: The temperature distribution across the strip was de-noised by means of the so-called shock-filter [40]. The de-noised temperature was denoted as $\hat{T}$.
- Step 2: The module of the temperature gradient was evaluated for each pixel of the IR picture of the graphene strip as follows:

$$g(i, j) = \sqrt{\left(\frac{\partial \hat{T}(i, j)}{\partial x}\right)^2 + \left(\frac{\partial \hat{T}(i, j)}{\partial y}\right)^2},\quad (8)$$

where (i, j) were the coordinates of the examined pixel.

- Step 3: The area A was identified as the largest rectangle for which $g(i, j) \leqslant 0.1$, as suggested in [41]. The upper bound value of 0.1 was obtained by the authors on the basis of numerical benchmarks.

The next step was the calculation of the convective heat transfer coefficient $h_n(\vartheta)$. To this end, besides the discretization in the y-direction reported in figure 6, the strip was divided in sub-strips in other planar direction (x-direction), so to obtain the following discretization:

$$0 \leqslant z \leqslant \delta, \ \frac{b - w}{2} \leqslant x \leqslant \frac{b + w}{2}, \ y_n \leqslant y \leqslant y_n + \Delta y,\quad (9)$$

where b (figure 5) and δ (figure 6) are the strip width and thickness, respectively. Since the analysis was based on the frames provided by the IR images, Δy was taken as the length of a vertical pixel and w is taken as a multiple value of the length of a horizontal pixel (in particular, here it was equal to 7 pixels).

For each of such sub-strips, a mean temperature value at the coordinate y_n was evaluated by solving the above model. This value, denoted as $\tilde{T}_n(\vartheta)$, was then used to estimate the air thermo-dynamical properties (such as the air temperature) from which it was possible to evaluate the value of $h_n(\vartheta)$ by following the approach introduced in [42]. Note that, having chosen a width of each sub-strip w smaller than b, the boundary effects in heat transfer can be neglected, being the boundaries of each sub-strip w along the x-direction almost adiabatic.

3. Results and discussion

3.1. Setup calibration and preliminary characterization

A preliminary study was performed at room temperature, with the aim of assessing the setup, evaluating and de-embedding
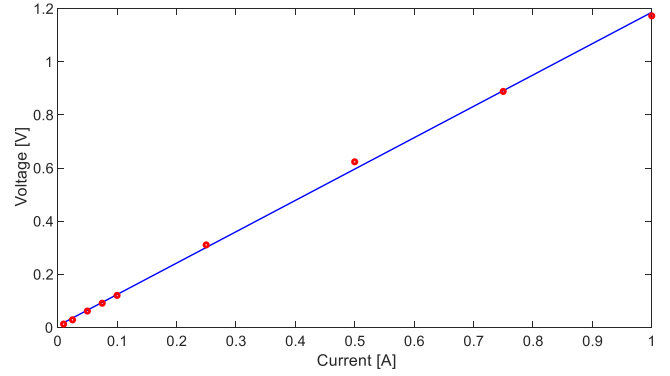

Figure 7. Linear *V–I* characteristic of a pure g-paper strip: red dots (measured values); blue curve (fitting).

Table 2. Fitting parameters for the linear model of the resistivity (10), at the reference temperature of 20 °C.

Material	ρ_0 (m/kS)	α (1/°C)
G-paper	7.8644×10^{-6}	-1.5452×10^{-3}
G-Preg (95/5)	1.5583×10^{-5}	-1.3761×10^{-3}
G-Preg (80/20)	2.0959×10^{-5}	-1.2236×10^{-3}
G-Preg (70/30)	2.3360×10^{-5}	-1.4468×10^{-3}
G-Preg (50/50)	5.3938×10^{-5}	-1.2601×10^{-3}
G-Preg (30/70)	1.7102×10^{-4}	-1.0542×10^{-3}
G-Preg (25/65-10)	9.5368×10^{-5}	-1.4009×10^{-3}

the setup parasitics, and verifying the linearity of the current–voltage (*I–V*) response of the graphene strips. Specifically, in view of using the Joule effect to heat the strip, the electrical resistance was measured by using the multimeter AGILENT 34400A with the four probes method, in order to exclude the contribution of the contact resistance due to the electrodes. Resistance values of the order of Ohms were found with satisfactory reproducibility and repeatability performance. Indeed, the standard deviation for 10 repeated measurements on the same sample was equal to 0.87 mΩ, and for the measurements on 10 different samples was 31.2 mΩ.

Next, by checking the voltage values corresponding to the known current values imposed by the power supply QJE QJ-3005A III, a linear *I–V* characteristic was verified (see figure 7) in the current range (0.01–1) A, for almost all the graphene materials listed in table 1. Indeed, for the G-Preg (30/70) and the G-Preg (25/65-10) strips the maximum current level was set to 0.5 A, due to the higher content of polymer.

Following the technique presented in [26], an electro-thermal characterization was also carried out by placing the strips inside a climatic chamber (ACS, Model DY110), to verify the dependence of the electrical resistance with the temperature in the range of (−40, +60) °C. Coherently with the results in [26], all the graphene composites investigated here showed a linear relation between the resistance and temperature with a negative derivative:

$$\rho_{eq} = \rho_0(1 + \alpha(T - T_0)),\quad (10)$$

with the fitting parameters reported in table 2 (referred to T_0 = 20 °C).

3.2. Uncertainty evaluation of the thermal parameters

The procedure adopted here to evaluate the uncertainties $u^2(\cdot)$ of the measured thermal properties follows the international standard in [43].

Under the hypotheses of uncorrelated uncertainties, the uncertainty on the value of $\rho \cdot c$ is given by the following relation:

$$u^2(\rho c) = \left(\frac{\partial (\rho c)}{\partial \delta}\right)^2 \cdot u^2(\delta) + \left(\frac{\partial (\rho c)}{\partial A}\right)^2 \cdot u^2(A)$$
$$+ \left(\frac{\partial (\rho c)}{\partial T_\infty}\right)^2 \cdot u^2(T_\infty) + \left(\frac{\partial (\rho c)}{\partial T_w}\right)^2 \cdot u^2(T_w) + \left(\frac{\partial (\rho c)}{\partial h}\right)^2$$
$$\times u^2(h) + \left(\frac{\partial (\rho c)}{\partial \varepsilon}\right)^2 \cdot u^2(\varepsilon) + \left(\frac{\partial (\rho c)}{\partial \tilde{T}}\right)^2 \cdot u^2(\tilde{T}).$$
$$\text{(11)}$$

Under the same assumption, the uncertainty on k is given by:

$$u^2(k) = \left(\frac{\partial k}{\partial w}\right)^2 \cdot u^2(w) + \left(\frac{\partial k}{\partial \delta}\right)^2 \cdot u^2(\delta)$$
$$+ \left(\frac{\partial k}{\partial A_n}\right)^2 \cdot u^2(A_n) + \left(\frac{\partial k}{\partial \Delta y}\right)^2 \cdot u^2(\Delta y)$$
$$+ \left(\frac{\partial k}{\partial T_\infty}\right)^2 \cdot u^2(T_\infty) + \left(\frac{\partial k}{\partial T_w}\right)^2 \cdot u^2(T_w)$$
$$+ \left(\frac{\partial k}{\partial h_n}\right)^2 \cdot u^2(h_n) + + \left(\frac{\partial k}{\partial \varepsilon}\right)^2 \cdot u^2(\varepsilon)$$
$$+ \left(\frac{\partial k}{\partial \Delta R_n}\right)^2 \cdot u^2(\Delta R_n) + \left(\frac{\partial k}{\partial I}\right)^2 \cdot u^2(I) + \left(\frac{\partial k}{\partial \tilde{T}}\right)^2 \cdot u^2(\tilde{T})$$
$$+ \left(\frac{\partial k}{\partial (\rho c)}\right)^2 \cdot u^2(\rho c) + u^2(\text{mesh}),$$
$$\text{(12)}$$

where $u^2(\text{mesh})$ is the uncertainty associated to the spatial discretization in figure 6.

In addition, from (1) and [42] the combined standard uncertainty for the thermal diffusivity can be written as:

$$u(a) = \sqrt{\left(\frac{1}{\rho c}\right)^2 \cdot u^2(k) + \left(-\frac{k}{(\rho c)^2}\right)^2 \cdot u^2(\rho c)}. \quad \text{(13)}$$

As for the uncertainty of the measured temperature $\tilde{T}$, the following relation holds:

$$u^2(\tilde{T}) = u^2(\tilde{T})_{\text{noise}} + u^2(\tilde{T})_{\text{uniformity}} + u^2(\tilde{T})_{\text{IR camera}}, \quad \text{(14)}$$

where $u(\tilde{T})_{\text{noise}}$ is evaluated on the basis of the mentioned de-noising procedure and it is equal to:

$$u(\tilde{T})_{\text{noise}} = \max \left(\frac{\tilde{T}_{\text{noisy}} - \tilde{T}_{\text{de-noised}}}{2\sqrt{3}}\right)_{\text{region}}, \quad \text{(15)}$$

whereas $u(\tilde{T})_{\text{uniformity}}$ is given by:

$$u(\tilde{T})_{\text{uniformity}} = \left(\frac{\tilde{T}_{\text{de-noised, max}} - \tilde{T}_{\text{de-noised, min}}}{2\sqrt{3}}\right)_{\text{region}}, \quad \text{(16)}$$

where 'region' is the uniformity area A previously defined. Typical values of $u(\tilde{T})$ are lower than 0.2 K.

3.3. Validation and limits of applicability of the method

The proposed methodology was validated by applying it to two GNP strips produced by Panasonic® and GrafTech®. The planar dimensions were 1.3 cm × 18 cm for both the strips, while the thicknesses were respectively 50 μm and 76 μm. The values of the parameters obtained with the proposed methodology are reported in table 3, compared with those declared by the manufacturers (when available). In particular, an excellent agreement was found in the evaluation of the thermal conductivity k, with a low percent relative error between measured and declared values, that was −0.6% and +0.3% for the Graftech and the Panasonic samples, respectively.

To estimate the limits of applicability of the proposed methodology, it has to be noted that the lower limits are dictated by the uncertainty rather than by the relative error. To investigate this point, tables 4 and 5 report the budgets of the combined standard uncertainty for k and $\rho \cdot c$ referred to the benchmark cases. The sources of uncertainties can be grouped in two categories: those related to the sample fabrication (such as, for instance, its thickness δ), and those related to the method (such as, for instance, the numerical discretization). In principle, the uncertainty due to the fabrication can be lowered at will paying the price of a more and more accurate preliminary morphological characterization of the sample. Instead, the second type of uncertainty sets the real limit of applicability of the method. As for the Panasonic sample, uncertainty values of 3.7% on k and of 9.7% on a were found, mainly due to the model (the most important contribution comes from the estimation of ρc). Instead, for the Graftech sample, higher values of uncertainties were found (14.8% on k and of 17.3% on a), but mainly associated to the fabrication uncertainties. As a general trend, also confirmed by the results shown in the following subsection 3.4, the uncertainty reduces for higher values of k and a. Therefore, the lower limits of validity are related to the maximum uncertainty which can be tolerated when low values of k and a are considered. Given the scope of this paper, a maximum uncertainty of 20% can be accepted, which is in line with the uncertainty values found in literature for similar methodologies, such as that in [34]. With this choice, the lower limits of applicability of the proposed method are equal to 150 W m^{-1} K^{-1} for the thermal conductivity k, and to 1.5×10^{-4} m^2 s^{-1} for the thermal diffusivity a.

As for the upper limits, they depend on the quality and performance of the IR camera. Indeed, higher values of k would require a better resolution and sensitivity, to properly estimate the thermal gradients across the sample, whereas higher values of a would require a higher frame-rate. Consequently, the upper limits could be increased by increasing

Table 3. Method validation, measured values versus those declared by manufacturers (some data are not available (NA)).

Parameter	Graftech (measured)	Graftech (declared)	Panasonic (measured)	Panasonic (declared)
ε	0.50	NA	0.60	NA
$u(\varepsilon)$	0.01	NA	0.01	NA
$k(\mathrm{W\,m^{-1}\,K^{-1}})$	497.2	500	1303.5	1300
$u(k)$ ($\mathrm{W\,m^{-1}\,K^{-1}}$)	73.5	NA	48.3	NA
$u(k)\%$	14.8	NA	3.7	NA
$a(\mathrm{m^2\,s^{-1}})$	3.03×10^{-4}	NA	7.93×10^{-4}	NA
$u(a)$ ($\mathrm{m^2\,s^{-1}}$)	5.22×10^{-5}	NA	7.67×10^{-5}	NA
$u(a)\%$	17.3	NA	9.7	NA

Table 4. Uncertainty budget for k.

	Graftech		Panasonic	
Parameter	$u^2(\bullet)$	$u^2(\bullet)/u^2(k) \times 100$	$u^2(\bullet)$	$u^2(\bullet)/u^2(k) \times 100$
T_n	4.75×10^2	8.79	6.09×10^{-5}	2.61×10^{-6}
T_w	1.08×10^1	0.199	2.13×10^{-9}	9.13×10^{-11}
T_∞	1.44×10^2	2.66	5.37×10^{-8}	2.30×10^{-9}
L	5.04×10^0	9.33×10^{-2}	7.44	0.318
b	1.61×10^1	0.298	1.20×10^{-8}	5.12×10^{-10}
δ	2.27×10^3	42.0	4.35×10^{-8}	1.86×10^{-9}
ε	8.82	0.163	4.08×10^{-8}	1.74×10^{-9}
ΔR_n	7.94×10^2	14.7	6.44×10^{-7}	2.76×10^{-8}
h_n	1.68×10^3	31.0	6.10×10^{-6}	2.61×10^{-7}
ρc	3.94×10^{-4}	7.30×10^{-6}	2.33×10^3	99.7

Table 5. Uncertainty budget for ρc.

	Graftech $\rho c = 2.32 \times 10^6$ J m^{-3} K^{-1} $u(\rho c) = 2.67 \times 10^5$ J m^{-3} K^{-1}		Panasonic $\rho c = 1.27 \times 10^6$ J m^{-3} K^{-1} $u(\rho c) = 1.09 \times 10^5$ J m^{-3} K^{-1}	
Parameter	$u^2(\bullet)$	$u^2(\bullet)/u^2(k) \times 100$	$u^2(\bullet)$	$u^2(\bullet)/u^2(k) \times 100$
T_n	3.41×10^{10}	47.8	5.29×10^8	4.47
T_w	3.61×10^8	0.506	1.62×10^8	1.37
T_∞	2.36×10^9	3.30	8.43×10^8	7.13
δ	7.85×10^9	11.0	2.81×10^9	23.8
ε	1.92×10^8	0.269	4.60×10^7	0.389
h_n	2.65×10^{10}	37.2	7.43×10^9	62.8

the cost of the experimental setup. Given the characteristics of the IR camera adopted here, the upper limit for k is equal to 1000 W m^{-1} K^{-1}, whereas the upper limit for a is equal to 8×10^{-4} m^2 s^{-1}.

Note that the values obtained here for the two benchmark samples fall in the validity range of the method.

3.4. Thermal characterization of GNP strips

The proposed methodology was applied to the GNP strips listed in table 1. Two thermal maps are reported in figure 8, showing the temperature distribution over the G-paper strip, at the initial time instant and at steady-state. The thermal transient is instead reported in figure 9, that plots the time evolution of the temperature measured at the central point of the strip. The transient evolution highlights the presence of a

fast thermal time-constant (in the order of seconds), as typical for graphene-related materials.

The results of the characterization are reported in tables 6 and 7. For the strips characterized by a low percentage of binder (from 0% to 30%), hence by a higher content of GNPs, the thermal conductivity k values range from 162.6 to 453.8 W m^{-1} K^{-1}. For the same strips, the values of the thermal diffusivity a fall in the range from 1.63×10^{-4} to 3.65×10^{-4} m^2 s^{-1}. Increasing the percentage of the binder to 50% and 65% (table 7) results in a significant decrease of k, in the range from 54.7 to 329.5 W m^{-1} K^{-1}, and of a, now in the range from 0.69×10^{-4} to 3.06×10^{-4} m^2 s^{-1}.

As expected, a global trend can be observed, with the thermal conductivity and diffusivity decreasing as the binder percentage increases, as shown in figures 10 and 11. However, the G-Preg (50/50) sample presents an anomalous behavior both for thermal conductivity and diffusivity,
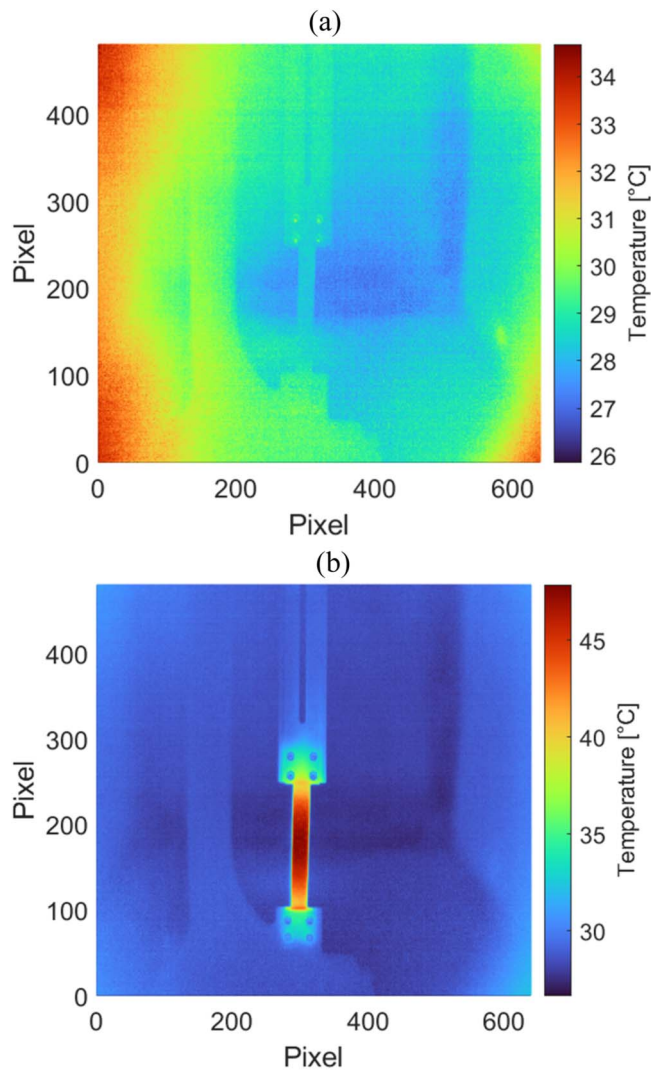
(a)

(b)

Figure 8. Temperature distribution over the G-paper strip at: (a) initial time instant; (b) steady state (thermal regime).
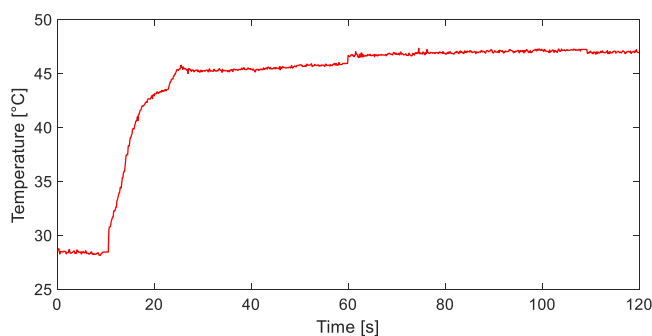

Figure 9. Thermal transient at the central point of the pure G-paper strip.

whereas the G-Preg (70/30) one only for the thermal diffusivity. Repeated measurements confirmed this behavior which can be probably associated to a non-uniform distribution of the binder in the considered samples. Morphological characterization of these samples will be carried out to further investigate this point.

Considering the analysis on the limits of applicability reported in subsection 3.3, the results in tables 6 and 7 are reliable for all the analyzed samples, except for G-Preg 30/70 and G-Preg (25/65-10), for which the uncertainties are too high, as also evident from figures 10 and 11.

Finally, some considerations are to be made on the estimation of the thermal emissivity. For such a parameter, no value has been provided by the manufacturers of the benchmark strips analyzed in table 3, whereas some results are available in [44] for the Nanesa samples G-paper and G-Preg (70/30), in a comparable spectral band (7.5–14 μm long wave) of the IR camera used in the present paper. The results obtained here are compared in table 8 to those reported in [44] showing a good agreement, given the uncertainties of fabrication of the samples.

4. Conclusions

This paper has proposed and validated a methodology to estimate the thermal conductivity and emissivity of thin graphene strips, based on the analysis of the spatial distribution and of the transient evolution of the temperature of the strips while heated by the Joule effect. Compared to existing standard techniques such as those based on Raman effects or laser-flash, the one proposed here is less demanding in terms of equipment, effort, and expertize, and therefore it candidates to implement a fast and low-cost and quality control stage in industrial fabrication processes. The main results obtained here are the following.

– The methodology has been successfully validated by applying it to two strips of GNPs produced by Panasonic® and GrafTech®, of dimensions 1.3 cm × 18 cm and thicknesses equal to were 50 μm and 76 μm, respectively. Compared to the values declared by the manufactures, the thermal conductivity k has been here estimated with a percent relative error equal to −0.6% and to 0.3% for the Graftech and the Panasonic sample, respectively.
– Strips of dimensions of 1 cm × 10 cm and thickness ranging from 65 to 100 μm have been analyzed, composed by pure GNPs or by GNPs mixed to different dielectric binders, produced by the manufacturer Nanesa®.
– GNP strips with a low percentage of binder (from 0% to 30%) have shown a thermal conductivity k in the range from 162.6 to 453.8 W m^{-1} K^{-1}, and a thermal diffusivity a in the range from 1.63×10^{-4} to 3.65×10^{-4} m^2 s^{-1}.
– GNP strips with a higher percentage of binder (from 50% and 65%) have instead shown a thermal conductivity k in the range from 54.7 to 329.5 W m^{-1} K^{-1}, and a thermal diffusivity a in the range from 0.69×10^{-4} to 3.06×10^{-4} m^2 s^{-1}.
– The lower limits of applicability of the proposed methodology depend on the maximum allowed uncertainty that has been here assumed to be 20%, in line with

Table 6. Measured thermal properties for pure GNP (G-paper) and for strips with a binder percentage from 5% to 30% (G-Preg).

Parameter	G-paper	G-Preg (95/5)	G-Preg (80/20)	G-Preg (70/30)
ε	0.50	0.53	0.80	0.56
$u(\varepsilon)$	0.01	0.01	0.01	0.01
k (W m^{-1} K^{-1})	453.8	295.5	268.5	162.6
$u(k)$ (W m^{-1} K^{-1})	67.6	51.5	56.3	41.3
$u(k)\%$	14.9	17.4	21.0	25.4
$u(k)\%$ method only	10.3	9.9	11.9	18.4
a (m^2 s^{-1})	3.65×10^{-4}	2.06×10^{-4}	1.63×10^{-4}	2.40×10^{-4}
$u(a)$ (m^2 s^{-1})	6.28×10^{-5}	4.06×10^{-5}	3.72×10^{-5}	6.39×10^{-5}
$u(a)\%$	17.2	19.8	22.8	26.6
$u(a)\%$ method only	12.3	12.5	13.9	19.6

Table 7. Measured thermal properties for strips with a binder percentage from 50% to 75% (G-Preg).

Parameter	G-Preg (50/50)	G-Preg (30/70)	G-Preg (25/65-10)
ε	0.70	0.75	0.82
$u(\varepsilon)$	0.01	0.01	0.01
k(W m^{-1} K^{-1})	329.5	54.7	86.0
$u(k)$ (W m^{-1} K^{-1})	44.9	73.9	63.0
$u(k)\%$	13.6	135.2	73.2
$u(k)\%$ method only	7.2	100.0	46.4
a(m^2 s^{-1})	3.06×10^{-4}	6.93×10^{-5}	1.09×10^{-4}
$u(a)$ (m^2 s^{-1})	4.91×10^{-5}	9.39×10^{-5}	8.04×10^{-5}
$u(a)\%$	16.1	135.6	73.8
$u(a)\%$ method only	10.0	100.0	46.8
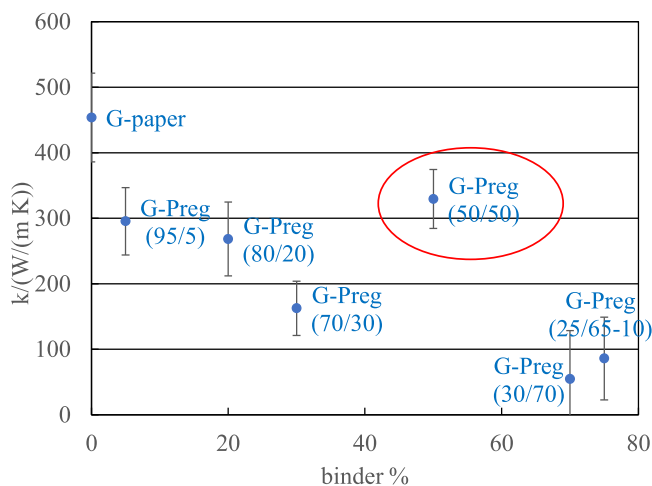
Figure 10. Estimated thermal conductivity values for the analyzed GNP strips versus the binder percentage.
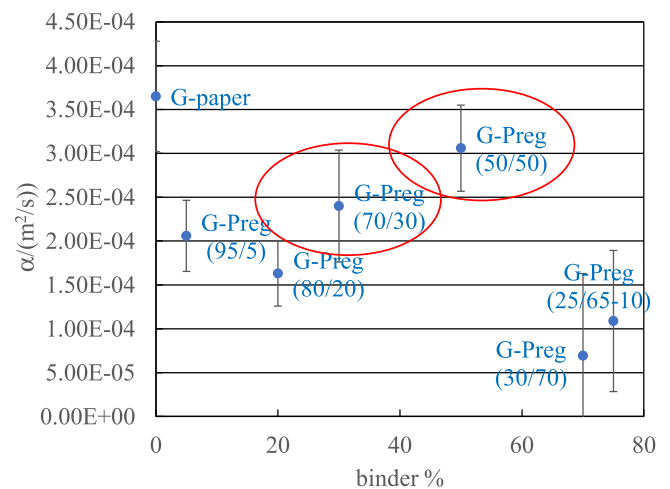
Figure 11. Estimated thermal diffusivity values for the analyzed GNP strips versus the binder percentage.

the values found in the literature for comparable methodologies. With this assumption, these lower limits have been estimated as 150 W m^{-1} K^{-1} for the thermal conductivity *k,* and as 1.5×10^{-4} m^2 s^{-1} for the thermal diffusivity *a*.

– The upper limits of applicability depend instead on the quality and performance of the IR camera. Given the equipment available here, the have been set to 1000 W m^{-1} K^{-1} for *k*, and to 8×10^{-4} m^2 s^{-1} for *a*.

The results obtained here suggest the use of this industrial-grade graphene for a large class of thermal and electro-thermal applications although it obviously does not exhibit those outstanding values of pure (but extremely expensive) graphene (e.g. a conductivity of 4000 W m^{-1} K^{-1}).

As a perspective work, the method will be further improved in order to lower the uncertainty related to the numerical scheme, and thus widening its validity range. Indeed, future works will implement a 2D (rather than a 1D)

Table 8. Values of the thermal emissivity estimated here, compared with the results in [44].

Sample	Emissivity (here)	Emissivity [44]
G-paper	0.50	0.40
G-Preg (70/30)	0.56	0.45

formulation of the numerical problem and thus the transverse distribution of the temperature will be more accurately simulated. This will reduce the uncertainty contribution due to the approximation of uniform temperature in the transverse section of the strips. Consequently, also the combined standard uncertainty in the evaluation of ρc and k will decrease. Moreover, other test setup configurations will be studied in order to measure also the off-plane component of the thermal conductivity.

Acknowledgments

Data availability statement

All data that support the findings of this study are included within the article (and any supplementary files).

Conflict of interest statement

The authors declare no conflict of interest.

Ethics statement

The authors declare no ethics issue.

Author contributions

G Giovinco (GG) and S Sibilia (SS) contributed equally to this work. GG: conceptualization, methodology, data analysis, manuscript writing. SS: methodology, experimental characterization, data analysis, manuscript writing. A Maffucci: fund raising, supervision, conceptualization, manuscript review. All authors discussed and interpreted the results.

ORCID iDs

G Giovinco ⓘ https://orcid.org/0000-0001-6779-5774
S Sibilia ⓘ https://orcid.org/0000-0001-7082-7570
A Maffucci ⓘ https://orcid.org/0000-0002-4992-9449

References

[1] Yan Z, Nika D L and Balandin A A 2015 Thermal properties of graphene and few-layer graphene: applications in electronics *IET Circuits Devices Syst.* **9** 4–12

[2] Janas D and Koziol K K 2014 A review of production methods of carbon nanotube and graphene thin films for electrothermal applications *Nanoscale* **6** 3037–45

[3] Jeong Y G and Jeon G W 2013 Microstructure and performance of multiwalled carbon nanotube/m-aramid composite films as electric heating elements *ACS Appl. Mater. Interfaces* **5** 6527–34

[4] Dui D, Huang Y, Huang L, Linag J, Ma Y and Chen Y 2011 Flexible and transparent electrothermal film heaters based on graphene materials *Small* **7** 3186–92

[5] Wang R, Xu Z, Zhuang J, Liu Z, Li Z, Liu Y, Gao W and Gao C 2017 Highly stretchable graphene fibers with ultrafast electrothermal response for low-voltage wearable heaters *Adv. Electron. Mater.* **3** 1600425

[6] Smovzh D V *et al* 2020 Joule heater based on single-layer graphene *Nanotechnology* **31** 335704

[7] Davaji B, Cho H D, Malakoutian M, Lee J-K, Panin G, Kang T W and Lee C H 2017 A patterned single layer graphene resistance temperature sensor *Sci. Rep.* **7** 8811

[8] Han S *et al* 2019 Thermally and electrically conductive multifunctional sensor based on epoxy/graphene composite *Nanotechnology* **31** 075702

[9] Koskinen T, Juntunen T and Tittonen I 2020 Large-area thermal distribution sensor based on multilayer graphene ink *Sensors* **20** 5188

[10] Huang P, Li Y, Yang G, Li Z-X, Li Y-Q, Hu N, Fu S-Y and Novoselov K S 2021 Graphene film for thermal management: a review *Nano Mater. Sci.* **3** 1–16

[11] Bae S H, Shabani R, Lee J B, Baeck S J, Cho H J and Ahn J H 2014 Graphene-based heat spreader for flexible electronic devices *IEEE Trans. Electron Devices* **61** 4171–5

[12] Vu M C *et al* 2021 Scalable ultrarobust thermoconductive nonflammable bioinspired papers of graphene nanoplatelet crosslinked aramid nanofibers for thermal management and electromagnetic shielding *J. Mater. Chem.* A **9** 8527–40

[13] Animasaun I L *et al* 2022 *Ratio of Momentum Diffusivity to Thermal Diffusivity: Introduction, Meta-analysis, and Scrutinization* (New York: Chapman and Hall/CRC)

[14] Tan Y W, Zhang Y, Stormer H L and Kim P 2007 Temperature-dependent electron transport in graphene *Eur. Phys. J.* **148** 15–8

[15] Forestiere C, Maffucci A and Miano G 2011 On the evaluation of the number of conducting channels in multiwall carbon nanotubes *IEEE Trans. Nanotechnol.* **10** 1221–3

[16] Balandin A 2011 Thermal properties of graphene and nanostructured carbon materials *Nat. Mater.* **10** 569–81

[17] Estrada D *et al* 2019 Thermal transport in layer-by-layer assembled polycrystalline graphene films *Npj 2D Mater. Appl.* **3** 10

[18] Khan M F, Shahil A and Balandin A 2012 Thermal properties of graphene and multilayer graphene: applications in thermal interface materials *Solid State Commun.* **152** 1331–40

[19] Forestiere C, Maffucci A and Miano G 2010 Hydrodynamic model for the signal propagation along carbon nanotubes *J. Nanophotonics* **4** 041695

[20] Kovtun A *et al* 2019 Benchmarking of graphene-based materials: real commercial products versus ideal graphene *2D Mater* **6** 025006

[21] Prolongo S G and Suárez A J 2020 *Graphene Nanoplatelets* (Basel, Switzerland: MDPI Publishing)

[22] Dabrowska A, Bellucci S, Cataldo A, Micciulla F and Huczko A 2014 Nanocomposites of epoxy resin with graphene nanoplates and exfoliated graphite: synthesis and electrical properties *Phys. Status Solidi* b **251** 2599–602

[23] Maffucci A, Micciulla F, Cataldo A, Miano G and Bellucci S 2016 Bottom–up realization and electrical characterization of a graphene-based device *Nanotechnology* **27** 095204

[24] Zhang H, Xu C, Xiao W, Ameyama K and Ma C 2016 Enhanced mechanical properties of Al5083 alloy with graphene nanoplates prepared by ball milling and hot extrusion *Mater. Sci. Eng.* A **658** 8–15

[25] Malik R *et al* 2020 Synthesis of layered silicon-graphene hetero-structures by wet jet milling for high capacity anodes in Li-ion batteries *2D Mater.* **8** 015012

[26] Sibilia S, Bertocchi F, Chiodini S, Cristiano F, Ferrigno L, Giovinco G and Maffucci A 2021 Temperature-dependent electrical resistivity of macroscopic graphene nanoplatelet strips *Nanotechnology* **32** 275701

[27] Lahbacha K, Sibilia S, Trezza G, Giovinco G, Bertocchi F, Chiodini S, Cristiano F and Maffucci A 2022 Electro-thermal parameters of graphene nano-platelets films for de-icing applications *Aerospace* **9** 107

[28] Fu Y 2020 Graphene related materials for thermal management *2D Mater.* **7** 012001

[29] Kim H G *et al* 2017 Effect of graphene-substrate conformity on the in-plane thermal conductivity of supported graphene *Carbon* **125** 39–48

[30] Potenza M, Cataldo A, Bovesecchi G, Corasaniti S, Coppa P and Bellucci S 2017 Graphene nanoplatelets: thermal diffusivity and thermal conductivity by the flash method *AIP Adv.* **7** 075214

[31] Bellucci S, Bovesecchi G, Cataldo A, Coppa P, Corasaniti S and Potenza M 2019 Transmittance and reflectance effects during thermal diffusivity measurements of gnp samples with the flash method *Materials* **12** 696

[32] Vozár L and Hohenauer W 2003 Flash method of measuring the thermal diffusivity. a review *High Temp.-High Press.* **35/36** 253–64

[33] ASTM E1461-13 2022 Standard Test Method for Thermal Diffusivity by the Flash Method (https://astm.org/e1461-13r22.html)

[34] Kabiri Samani M, Lu C, Qinyu K, Khosravian N, Chen G, Tan C, Rudquist P, Tay B K and Liu J 2019 Thermal conductivity enhancement of carbon@ carbon nanotube arrays and bonded carbon nanotube network *Mater. Res. Express* **6** 085616

[35] https://www.nanesa.it/graphene-flagship/

[36] Bejan A and Kraus A D 2003 *Heat Transfer Handbook.* (New York: Wiley)

[37] Tian X, Itkis M E, Bekyarova E and Haddon R 2013 Anisotropic thermal and electrical properties of thin thermal interface layers of graphite nanoplatelet-based composites *Sci Rep.* **3** 1710

[38] Özişik M N, Orlande H R B, Colaço M J and Cotta R M 2017 *Finite Difference Methods in Heat Transfer* 2nd edn (Boca Raton, FL: CRC Press) (https://doi.org/10.1201/9781315121475)

[39] Maffucci A, Ferrigno L, Sibilia S, Bertocchi F, Chiodini S, Cristiano F and Giovinco G 2021 Electrothermal modeling and characterization of graphene-based thin strips *25th IEEE Workshop on Signal and Power Integrity, SPI 2021 (Siegen, Germany, 10-12 May 2021)* paper #28 (https://doi.org/10.1109/SPI52361.2021.9505177)

[40] Gilboa G, Sochen N A and Zeevi Y Y 2002 Regularized shock filters and complex diffusion *Computer Vision-ECCV 2002 7th European Conf. on Computer Vision* vol 200228-21 May 2002 ed A Heyden, G Sparr, M Nielsen and P Johansen (London: Springer) pp 399–413 Copenhagen, Denmark, Proc. Part I

[41] Seibold P 2020 Largest inscribed rectangle square or circle, MATLAB Central File Exchange (https://it.mathworks.com/matlabcentral/fileexchange/71491-largest-inscribed-rectangle-square-or-circle)

[42] Churchill S W and Chu H H S 1975 Correlating equations for laminar and turbulent free convection from a vertical plate *Int. J. Heat Mass Transfer* **18** 1323–9

[43] ISO/IEC Guide 98-3 2008 Uncertainty of measurement – Part 3: Guide to the expression of uncertainty in measurement (GUM:1995) (https://www.iso.org/standard/50461.html)

[44] Leone C, Genna S, Bertocchi F, Giordano M and Martone A 2021 A procedure to measure the emissivity of ultra-thin graphene based film in long wavelength infrared (LWIR) spectrum region *Opt. Laser Technol.* **138** 106910